PAPER

Role of plasma response in displacements of the tokamak edge due to applied non-axisymmetric fields

To cite this article: N.M. Ferraro et al 2013 Nucl. Fusion **53** 073042

View the article online for updates and enhancements.

Role of plasma response in displacements of the tokamak edge due to applied non-axisymmetric fields

N.M. Ferraro[1], T.E. Evans[1], L.L. Lao[1], R.A. Moyer[2], R. Nazikian[3], D.M. Orlov[2], M.W. Shafer[4], E.A. Unterberg[4], M.R. Wade[1] and A. Wingen[4]

[1] General Atomics, PO Box 85608, San Diego, CA 92186-5608, USA

[2] Center for Energy Research, University of California San Diego, 9500 Gilman Drive, La Jolla, CA 92093-0417, USA

[3] Princeton Plasma Physics Laboratory, PO Box 451, Princeton, NJ 08543-0451, USA

[4] Oak Ridge National Laboratory, PO Box 2008, Oak Ridge, TN 37831, USA

E-mail: ferraro@fusion.gat.com

Abstract
Linear, two-fluid, resistive modelling of the plasma response to applied non-axisymmetric fields shows significant displacement of edge temperature and density profiles. The calculated displacements, often of 2 cm or more in H-mode pedestals with parameters appropriate to DIII-D, are due to the helical distortions resulting from stable edge modes being driven to finite amplitude by the applied fields. In many cases, these displacements are greater in magnitude, and different in phase, than the distortions of the separatrix manifolds predicted from vacuum modelling. Comparison of these results with experimental measurements from Thomson scattering and soft x-ray imaging finds good quantitative agreement. In these experiments, the phase of the applied non-axisymmetric magnetic field was flipped or rotated in order to probe the non-axisymmetric features of the response. The poloidal structures measured by x-ray imaging show clear indications of a helical response, as opposed to simply a change in the axisymmetric transport. Inclusion of two-fluid effects and rotation are found to be important in obtaining quantitative agreement with Thomson scattering data. Modelling shows screening of islands in the H-mode pedestal, but island penetration near the top of the pedestal where the electron rotation vanishes in plasmas with co-current rotation. Enhanced transport due to these islands may provide a mechanism for maintaining the pedestal width below the stability threshold of edge-localized modes. For typical DIII-D parameters, it is shown that the linear approximation is often near or beyond the limit of validity in the H-mode edge; however, the general agreement with experimental measurements indicates that these linear results nevertheless maintain good predictive value for profile displacements.

(Some figures may appear in colour only in the online journal)

1. Introduction

The application of non-axisymmetric magnetic fields in tokamaks is observed to affect the performance of the plasmas significantly, even when the non-axisymmetric fields are a small fraction ($\sim 10^{-4}$–10^{-3}) of the axisymmetric fields present in the device. Judicious application of non-axisymmetric fields may improve plasma performance by supporting toroidal rotation of the plasma [1], which is generally stabilizing, or by mitigating or suppressing edge-localized modes (ELMs) [2]. Potentially deleterious effects are also often observed, such as a strong reduction in plasma density [3, 4] ('pump-out'), a reduction in mode-locking thresholds [5], and substantial distortions of the plasma edge [6–10]. In DIII-D, the peak-to-peak magnitude of these distortions, as measured by displacements of the temperature and density profiles, is often of order 1 cm on the low-field side of the plasma for typical ELM-suppression parameters with toroidal mode number $n = 3$, and may exceed 3 cm for $n = 1$ fields. For high performance ITER scenarios, which are now designed to have an outer gap of ~ 10 cm [11, 12], scaling the edge displacement with the linear dimensions of the device implies the possibility of direct or near contact of the scrape-off layer (SOL) with the first wall

Here, we calculate the plasma response to applied non-axisymmetric fields from a linear, two-fluid, resistive model using the M3D-C1 code [13–15]. Essentially, these are linear perturbed equilibrium calculations similar to those

computed in several previous studies which considered ideal [16] and resistive [17] magnetohydrodynamic (MHD) response to non-axisymmetric fields using the IPEC [16] and MARS [18] codes. M3D-C1 is well-suited to the study of the edge response because its relatively comprehensive two-fluid model, discussed in section 2, includes diamagnetic effects which are important in the H-mode edge, and includes the separatrix and open field-line region even in diverted geometries. The linear response includes both the non-axisymmetric magnetic and thermal perturbations self-consistently, but not the associated changes to the axisymmetric equilibrium.

We find that the calculated thermal perturbations, which are essentially due to the displacement of magnetic surfaces, are in good agreement with experimental measurements of the plasma edge. In these experiments, a non-axisymmetric magnetic field is applied from the DIII-D I-coils, which are composed of two rows of six coils each, inside the vacuum vessel [19]. The toroidal phase of the applied non-axisymmetric fields is rotated (in the case of $n = 1$) or flipped (in the case of $n = 3$). Given an axisymmetric equilibrium in the absence of the non-axisymmetric fields, the difference between the measurements in the two phases must be indicative of the non-axisymmetric response, even if an $n = 0$ response is also present. In practice, the presence of error fields complicates this view. This possibility is discussed in section 4.

These perturbations are also found to be significantly enhanced by the plasma response to the non-axisymmetric fields in some cases. Although the lobe structure caused by the non-axisymmetric fields is qualitatively well described without taking into account the effect of the plasma response [8, 9], the measured displacements within the last closed flux surface (LCFS) may exceed the predictions of vacuum modelling by a factor of two or more [10, 20]. Indeed, it is found here that obtaining quantitative agreement with both the phase and magnitude of the measured displacement requires taking both equilibrium rotation and two-fluid effects into account in the calculation of the plasma response. Finally, it is shown that two-fluid response calculations predict screening of islands in the H-mode pedestal, where the electron rotation is large due to the diamagnetic drift, but the islands are typically amplified by the plasma near the top of the pedestal, where the electron rotation is relatively small. This sensitivity of the tearing response of the plasma to the electron rotation is consistent with previous two-fluid theory [21, 22] and modelling [15, 23, 24]. The enhancement of islands near the top of the pedestal provides a potential mechanism for constraining the pedestal width to a level that is stable to ELMs [25, 26].

2. Model

The model implemented in M3D-C1 includes the full plasma, separatrix, and SOL within its computational domain. The region outside the separatrix is treated as a low temperature, low density plasma. Density, temperature, and current density vary smoothly across the separatrix. The fluid velocity and pressure perturbations are zero at the simulation domain boundary. The simulation domain boundary, illustrated in figure 1, is well outside of the separatrix. The model under
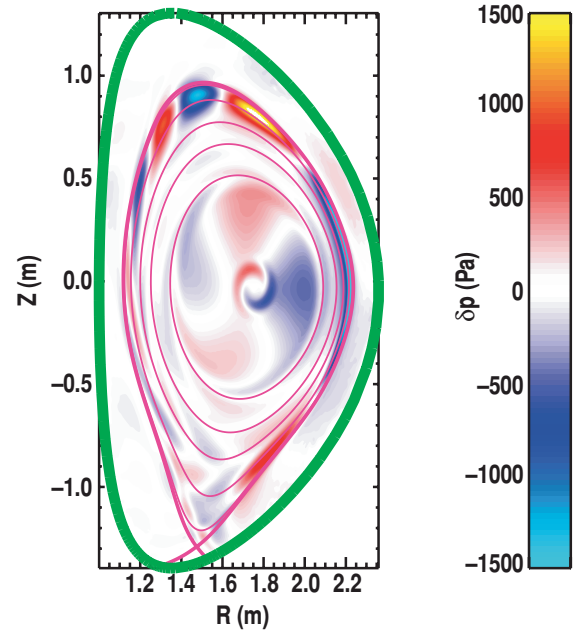
Figure 1. The modelled pressure perturbation due to the linear plasma response to 2 kA I-coil currents in an $n = 1$ configuration, using a reconstructed equilibrium from DIII-D discharge 117327 at toroidal angle $\varphi = 30°$ (in DIII-D machine coordinates). The thick green line indicates the simulation domain boundary. The magenta lines indicate the mode-rational surfaces with $q = 2$–6 and the separatrix.

consideration here is a set of time-independent two-fluid equations:

$$0 = \nabla \cdot (n_i \vec{v}), \tag{1}$$

$$0 = m_i n_i \vec{v} \cdot \nabla \vec{v} - \vec{J} \times \vec{B} + \nabla p + \nabla \cdot \Pi, \tag{2}$$

$$0 = \frac{1}{\Gamma - 1} \nabla \cdot (p\vec{v}) + p \nabla \cdot \vec{v} + \nabla \cdot \vec{q} - \eta J^2$$
$$+ \Pi : \nabla \vec{v} - \frac{1}{n_e e} \vec{J} \cdot \left(\frac{n_e \nabla T_e}{\Gamma - 1} - T_e \nabla n_e \right), \tag{3}$$

$$0 = \nabla \times \vec{E}, \tag{4}$$

where

$$\vec{J} = \nabla \times \vec{B}, \tag{5}$$

$$\vec{E} = \eta \vec{J} - \vec{v} \times \vec{B} + \frac{1}{n_e e} \left(\vec{J} \times \vec{B} - \nabla p_e \right), \tag{6}$$

$$\Pi = -\mu \left[\nabla \vec{v} + (\nabla \vec{v})^t \right], \tag{7}$$

$$\vec{q} = -\kappa \nabla (T_e + T_i) - \kappa_\parallel \vec{B}(\vec{B} \cdot \nabla T_e)/B^2. \tag{8}$$

In order to make quantitative comparisons with experimental density profiles, we assign the ion species a fractional charge equal to the 'effective' ionization state, Z, determined experimentally in the plasma edge, so that $n_e = Z n_i$. The ion mass is taken to be that of deuterium. Unless otherwise specified, we take $\kappa_\parallel/\kappa = 10^6$, and both κ and μ are taken to be constant and uniform such that $\kappa/n_i = \mu/n_i \approx 5\,\text{m}^2\,\text{s}^{-1}$ at the magnetic axis. The perturbed electron pressure is taken here to be half of the perturbed total pressure.

The input to M3D-C1 includes the reconstructed Grad–Shafranov equilibria of the discharges to be analysed, including axisymmetric electron temperature, electron density, and toroidal rotation profiles. In cases where equilibrium rotation

is included, the equilibrium is self-consistently modified to take this rotation into account by including poloidal variations in the equilibrium pressure and density profiles. In the calculations presented here, we have made the approximation that the equilibrium main ion rotation is entirely toroidal. The toroidal rotation profiles used here are inferred from charge exchange recombination (CER) spectroscopy measurements of the discharges being analysed [27]. While the ion rotation is taken to be purely toroidal, the electron velocity, determined in this model by

$$\vec{v}_{e} = \vec{v} - \frac{\vec{J}}{n_{e}e}, \tag{9}$$

has both toroidal and poloidal components. This relation naturally includes the diamagnetic components of the velocity. Since $\vec{J} \times \vec{B} \approx \nabla p$ in the axisymmetric equilibrium (this relation is not exactly satisfied due to small contribution of the centrifugal force), the components of $\vec{v}$ perpendicular to $\vec{B}$ differ from $\vec{v}_{e}$ by approximately the diamagnetic velocity $\vec{B} \times \nabla p / n_{e} e B^{2}$.

The currents in non-axisymmetric coils are also given as input. In the results presented here, the DIII-D I-coils are approximated as curved rectangles extending exactly $60°$ toroidally (whereas there are small toroidal gaps between coils in reality). The non-axisymmetric fields produced by these idealized I-coils are calculated using the Biot–Savart law. The component of these fields normal to the simulation domain boundary is held fixed as a boundary condition for the plasma response calculation. Thus, the domain boundary is treated as a perfect conductor which excludes the magnetic fields generated by the plasma. The boundary conditions used here are dictated by present limitations of the M3D-C1 code. Some potential consequences of this choice of boundary condition are discussed in section 4.

The linear plasma response is calculated by linearizing equations (1) through (3) and solving subject to the boundary conditions, as described in [15]. The outputs of the calculation are the perturbed density, pressure, velocity, and magnetic field of the solution. The linear calculations presented here include only the response having the same toroidal mode number as the applied field. The axisymmetric ($n = 0$) response is not considered.

3. Results

3.1. Edge displacements: $n = 1$

In DIII-D, one may smoothly vary the phase of an applied $n = 1$ field from the I-coils, which have six coils toroidally. This admits the possibility to resolve the toroidal structure of the resulting non-axisymmetric equilibrium by rotating it past the diagnostics. This method was applied in DIII-D discharge 117327, a diverted H-mode plasma which had the following parameters (with the usual definitions): $B_{T0} = -2.0\,\mathrm{T}$, $I_{p} = 1.1\,\mathrm{MA}$, $\beta_{N} = 1.66$, $q_{0} = 1.05$ and $q_{95} = 5.16$. In this case, $n = 1$ fields were applied with a 2 kA amplitude current waveform in the I-coils, and the waveform of the lower I-coil row was offset by $300°$ from the upper row. The toroidal phase of this field (both upper and lower I-coil rows together) was rotated at 5 Hz.
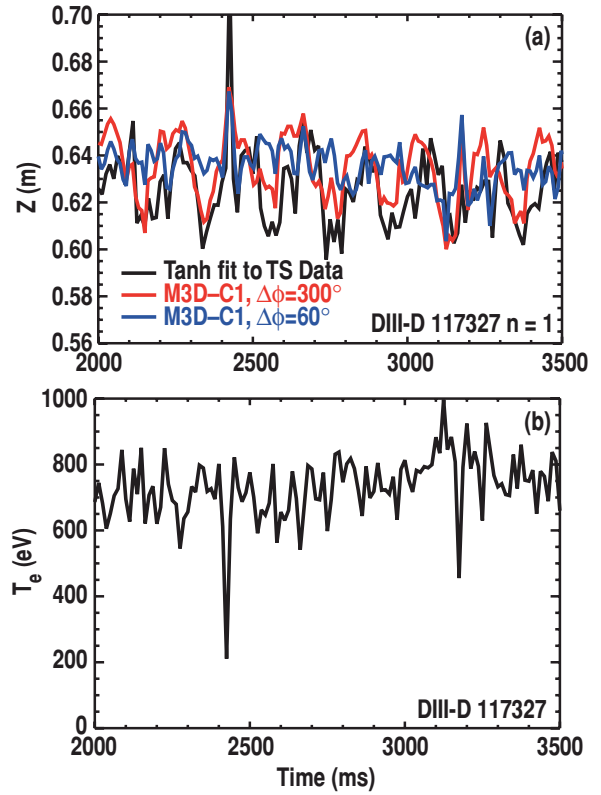
Figure 2. (*a*) The measured (black line) and modelled (red line) position of the top of the pedestal in DIII-D discharge 117327 along the core Thomson chord as an $n = 1$ perturbation from the I-coils is rotated at 5 Hz. The spikes at $t \approx 2400\,\mathrm{ms}$ and $t \approx 3150\,\mathrm{ms}$ are associated with ELMs. (*b*) The temperature of the pedestal top, T_{ped}, determined by tanh fits to the experimental data at each Thomson pulse.

Electron temperature and density data was collected along a vertically oriented chord using the DIII-D core Thomson scattering diagnostic, which is positioned at $R = 1.94\,\mathrm{m}$ and $120°$ in toroidal machine angle [28]. This system is designed to give optimal resolution near where this chord intersects the pedestal, which is approximately $Z = 0.64\,\mathrm{m}$ above the horizontal midplane in this case. In this discharge, which was carried out before the recent DIII-D Thomson upgrade [29], the spatial resolution along the chord was approximately 12 mm, and data was collected every 12.5 ms (80 Hz). For Thomson measurement, the electron temperature data is fit by a modified hyperbolic tangent function as described in [30]. Specifically, the fitting function is

$$T_{fit}(Z) = \frac{(1 + \alpha\zeta)e^{\zeta} - e^{-\zeta}}{e^{\zeta} + e^{-\zeta}}, \tag{10}$$

where $\zeta = (Z_{sym} - Z)/W$, and where α, Z_{sym}, and W are the fitting parameters. The position of the top of the pedestal, Z_{ped}, is defined as $Z_{ped} = Z_{sym} - W$. The electron temperature at the top of the pedestal is defined as $T_{ped} = T_{fit}(Z_{ped})$.

As the phase of the applied field was rotated, Z_{ped}, shown as the black line in figure 2(*a*), was observed to oscillate at the same frequency, as would be expected if a non-axisymmetric displacement were being rotated toroidally past the core Thomson diagnostic. The value of the measured electron temperature at the pedestal top, T_{ped}, is shown in figure 2(*b*).
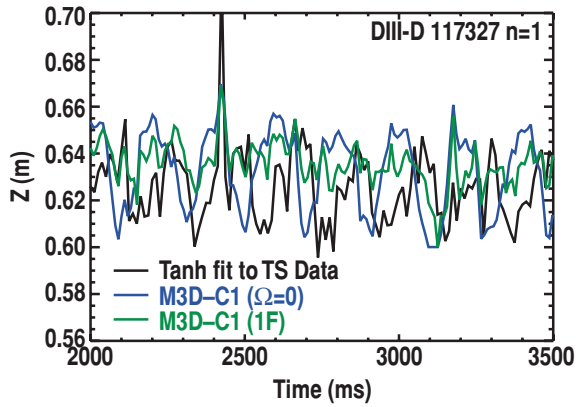
Figure 3. Neither a two-fluid M3D-C1 calculation that excludes the equilibrium toroidal rotation (blue line), nor a single-fluid M3D-C1 calculation (green line) reproduce the observed displacement as accurately as the two-fluid model with rotation (see figure 4(*a*)).

T_{ped} is roughly 700 eV, but there is significant noise due to fluctuations in the Thomson signal. T_{ped} apparently does not oscillate significantly with the frequency of the applied field.

To provide the equilibrium used to model this shot, the equilibrium was reconstructed using the experimentally determined pressure profile together with motional Stark effect measurements of the magnetic pitch. The response was calculated by doing a single linear M3D-C1 calculation to obtain the phase and magnitude of the plasma response for a given I-coil phase. The predicted Z_{ped} at any time t was then obtained simply by multiplying this result by the appropriate phase factor, and determining where the resulting T_e profile along the core Thomson chord equals the experimentally obtained $T_{ped}(t)$. This result is plotted versus time as the red line in figure 2(*a*), and is found to be in good agreement with the experimental results. In particular, both the phase and magnitude of the oscillation, which are not free parameters of the model, are found to be in good agreement.

These calculations were repeated using different assumptions in order to assess the sensitivity of these results to various parameters. First, a case excluding the equilibrium toroidal ion rotation was considered. In this case, shown as the blue line in figure 3, it is found that the magnitude of the displacement remains roughly consistent with the experimentally observed magnitude, but the phase of the response is no longer in agreement. In contrast, increasing the toroidal rotation by a factor of two over the experimental profile is found to have very little impact on the phase and magnitude of the displacement. Second, a case in which the two-fluid terms in the model were omitted was considered. In this single-fluid model, the magnitude of the displacement (green line in figure 3 is found to be significantly smaller than the observed displacement. Third, a case was run with purely isotropic thermal conductivity. The phase and magnitude of the displacements in this case do not differ significantly from the baseline two-fluid case, for which $\chi_{\parallel}/\chi_{\perp} = 10^6$. Finally, increasing the perpendicular diffusion coefficients (thermal diffusion and viscosity) together by a factor of ten is found to reduce the magnitude of the calculated displacement by roughly a factor of three; however, reducing these parameters by a factor of ten does not significantly change the magnitude or phase relative to the baseline case. Since the

perpendicular viscosity and thermal conductivity inferred from the measure profiles are generally somewhat smaller than those used in the baseline case ($\sim$5–10 m^2 s^{-1} throughout most of the plasma), we believe the displacements are well converged with respect to these parameters (although other features of the plasma response, such as magnetic island width and linear layer width, may depend on the specific values chosen).

3.2. Edge displacements: $n = 3$

Unlike $n = 1$ and $n = 2$ perturbations, the phase of $n = 3$ perturbations cannot be rotated smoothly using the DIII-D I-coils, which have 6 toroidal segments. Instead, the $n = 3$ response may be probed by reversing the I-coil currents, which would have the effect of reversing the sign of the $n = 3$ plasma response in the absence of error fields. This procedure was carried out in DIII-D discharge 148712, by reversing the 4 kA currents in the I-coils at 10 Hz. This discharge was a diverted H-mode plasma with the following parameters: $B_{T0} = -2.0$ T, $I_p = 1.6$ MA, $\beta_N = 1.73$, $q_0 = 0.97$, and $q_{95} = 3.55$. Thomson scattering measurements reveal a displacement of the edge T_e profile along the core Thomson chord of 1–1.5 cm through much of the H-mode pedestal. (This discharge followed the recent DIII-D Thomson upgrade, and had a spatial resolution of 6 mm [29].) These results are well reproduced by the M3D-C1 calculations, shown in figure 4. The equilibrium used here was based on data from the -4 kA phase, so there is a systematic shift of the modelling results to higher Z, but both the phase and magnitude of the modelled displacements are in good agreement with the experimental results through most of the pedestal. There is some discrepancy near the pedestal top, where the M3D-C1 result overestimates the size of the displacement. The calculated response is large here due to the vanishing of the electron rotation frequency ω_e in this region [15, 21, 24]. The linear approximation used here is likely no longer valid in the vicinity of this large response, as evidenced by the non-monotonic calculated temperature profile in the +4 kA case (this is discussed in section section 3.4).

The poloidal structure of the plasma response near the active x-point of DIII-D discharge 148712 is shown in figure 5. In this figure, the simulated x-ray signal given the perturbed density and temperature fields from M3D-C1 is compared with data from a soft x-ray diagnostic that has recently been upgraded on DIII-D [9, 31]. The plotted image is the difference between the x-ray signal averaged over a $\sim$75 ms period with the I-coils in one phase and over a similar period with the I-coil current reversed. The x-ray emissivity of the plasma edge has not yet been fully characterized, but it is known to be a strong function of the electron density. A 3 μm beryllium filter on the detector excludes low-energy x-rays, with roughly 8% transmission at 500 eV and 72% transmission at 1 keV. Although this discharge is ELMing, the contribution to the averaged signal from x-rays emitted during ELMs is negligible due to the infrequence and short duration (approximately tens of ms) of the ELMs relative to the integration time.

In both the M3D-C1 and soft x-ray results the edge response is seen to have a coherent and oscillatory poloidal structure. The poloidal structure in both results is consistent with a field-aligned mode structure in the edge. Both results
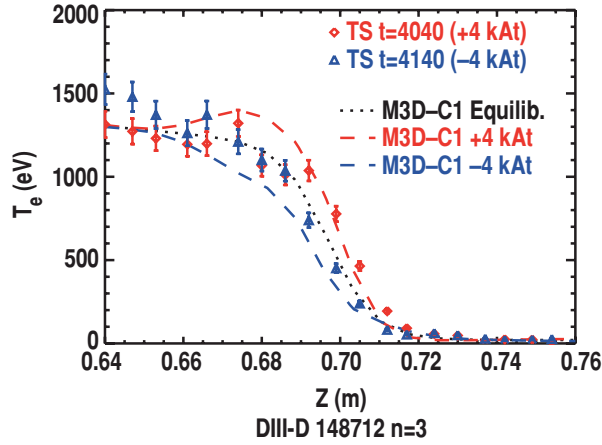
Figure 4. The data points show the measurement of T_e from Thomson scattering, in the presence of a +4 kA (red) and −4 kA (blue) $n = 3$ current in the I-coils in DIII-D discharge 148712. The T_e profiles calculated by M3D-C1 in the presence of these applied fields are shown by the coloured dashed lines. The black dotted line is the axisymmetric equilibrium input to M3D-C1.

also show strong radial localization, although it is not presently known to what extent the localization of the x-ray signal is due to the emissivity profile or the x-ray energy filtering, as opposed to the underlying mode structure.

3.3. Island formation and screening in the plasma edge

Due to the large anisotropic thermal conductivity in these calculations ($\chi_\parallel/\chi_\perp \sim 10^6$), the displacements of the temperature profile are largely indicative of the displacements of the magnetic surfaces. However, due to the presence of resistivity, there is no guarantee that magnetic surfaces are preserved in the perturbed solution. Indeed, it is found that both magnetic islands and stochasticity exist in these solutions. Because the rotating plasma tends to screen the magnetic islands [32], the islands are generally smaller than would be present if the perturbed fields were simply the applied fields (the 'vacuum' fields). Analytic theory [21, 22] and modelling [15, 23, 24] results have found that the degree of this reduction is sensitive to the rotation frequency of the plasma, and the perpendicular electron rotation in general. The perpendicular electron rotation frequency ω_e is defined by the standard non-orthogonal decomposition of the equilibrium electron velocity $\vec{v}_e = R^2 \omega_e(\psi)\nabla\varphi + [K(\psi)/n_e]\vec{B}$. In these calculations, the $\vec{E} \times \vec{B}$ drift frequency, $\omega_{E \times B} = \vec{E} \times \vec{B}/Rn_e eB^2$, is taken to be the profile inferred from CER spectroscopy [27]. The perpendicular ion and electron rotations are related to $\omega_{E \times B}$ through radial force balance: $\omega_{e,i} = \omega_{E \times B} + \omega_{*e,i}$, where $\omega_{*e} = -(\mathrm{d}p_e/\mathrm{d}\psi)/n_e e$ and $\omega_{*i} = (\mathrm{d}p_i/\mathrm{d}\psi)/n_e e$. The rotation profiles used in the simulation of DIII-D discharge 148712 are shown in figure 6.

Consistent with previous modelling results [15, 23, 24], the islands are found to be reduced in size in regions where $|\omega_e|$ is large, but enhanced in regions where $|\omega_e|$ is small ($\lesssim 10 \, \mathrm{krad \, s^{-1}}$). The resonant component of the normal magnetic field perturbations at each mode-rational surface, defined by

$$B_{mn}(\psi) = \frac{(2\pi)^2}{A} \int_0^{2\pi} \mathrm{d}\varphi \int_0^{2\pi} \mathrm{d}\theta \, \frac{\delta\vec{B} \cdot \nabla\psi}{\vec{B}_0 \cdot \nabla\theta} e^{\mathrm{i}(m\theta + n\varphi)}, \quad (11)$$
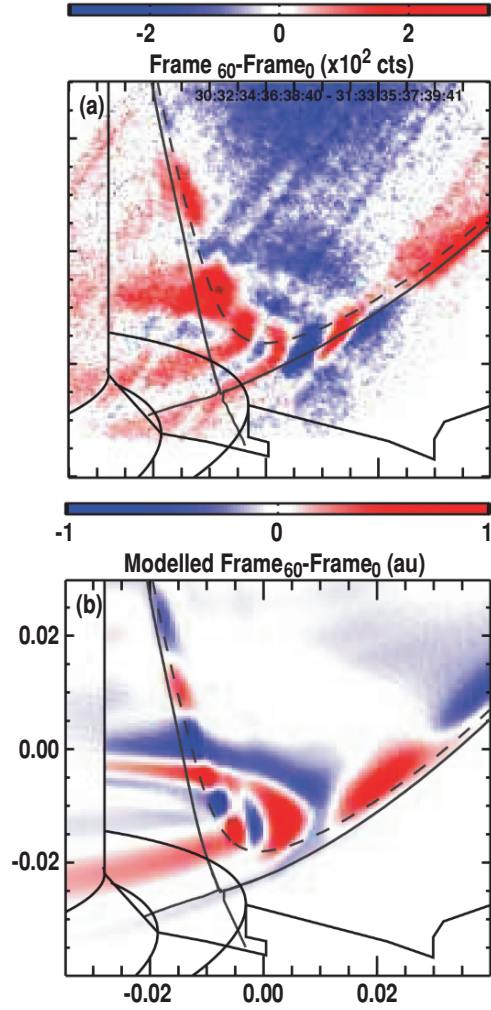
Figure 5. (*a*) The difference in the measured soft x-ray signal in response between opposite phases of applied $n = 3$ fields from the I-coils in DIII-D discharge 148712. (*b*) The simulated signal using temperature and density data from an M3D-C1 simulation of the same DIII-D discharge, using a model for x-ray emission. The dashed line represents the location of $\Psi = 0.98$.

where $m = nq(\psi)$, is proportional to the square of the island width [33]. The effect on the resonant components of the field due to the plasma response is illustrated in figure 7. Because of the reduction in the island width in the pedestal region, where the diamagnetic drift results in a large electron rotation, the magnetic stochasticity in that region is significantly reduced below what it would be in the absence of plasma response. In this simulation of 148712, the fraction of magnetic field lines that reach the simulation domain boundary within 200 toroidal transits, when followed from initial positions evenly distributed on the equilibrium $\Psi = 0.94$ surface (where Ψ is the normalized poloidal flux, with $\Psi = 0$ at the magnetic axis and $\Psi = 1$ at the separatrix), is reduced from more than 20% in the absence of plasma response to less than 5% when plasma response is included. Thus, while the linear plasma response is not sufficient to preserve closed magnetic surfaces in the pedestal in this case, it does significantly reduce the radial transport due to parallel thermal diffusion in the pedestal [34].

In contrast, the islands (and associated stochasticity) are found to be enhanced where ω_e is small; in this case,
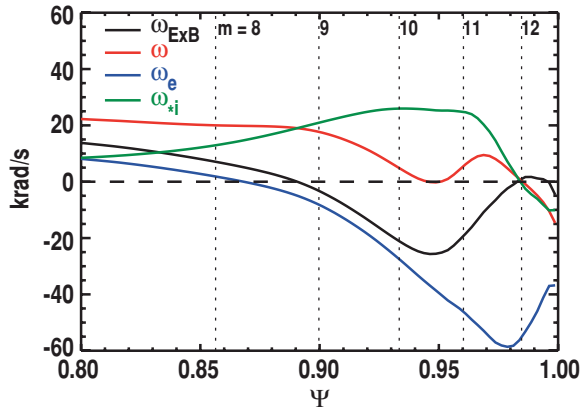
Figure 6. The equilibrium perpendicular ion rotation frequency (red), perpendicular electron rotation frequency (blue), $\vec{E} \times \vec{B}$ drift frequency (black), and ion diamagnetic drift frequency (green) used in the simulation of DIII-D discharge 148713. The $\vec{E} \times \vec{B}$ frequency was inferred from CER measurements. Vertical dotted lines indicate the locations of mode-rational surfaces.
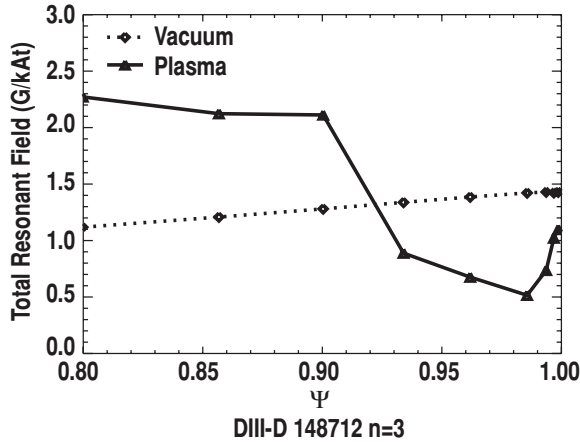
Figure 7. The magnitude of total resonant component of the perturbed normal magnetic field at each mode-rational surface from $q = 7/3$ ($\Psi \approx 0.8$) to $q = 15/3$ ($\Psi \approx 1.0$). The resonant fields (and hence also the island widths) including plasma response (triangles) are reduced below their values in the vacuum case (diamonds) except at the $q = 7/3$–$10/3$ surfaces, where $|\omega_e| \lesssim 10 \, \text{krad s}^{-1}$.

at the $q = 7/3$, $8/3$ and $9/3$ resonant surfaces. This enhancement presumably increases the radial thermal transport due to parallel diffusion, although this has not yet been quantified. This result suggests a potential mechanism for ELM suppression by applied non-axisymmetric fields, in which the enhanced transport due to these islands halts he expansion of the pedestal before the plasma becomes ELM-unstable.

3.4. Validity of linear model

The centimetre-scale displacements observed in the experimental results and in the calculations presented here are on the same scale as the equilibrium gradient scale lengths in the H-mode edge. This raises the concern that the assumption of linearity used here may be violated.

In the ideal-MHD response, magnetic surfaces remain intact, and the local linear displacement $\vec{\xi} = \int \vec{v} \, dt$ provides

a local measure of the physical displacement of these surfaces due to the response. As $\vec{\xi}$ becomes large, the local linear displacement may deviate from the actual geometry of the perturbed surfaces (as determined by field-line integration, for example). Additionally, sharp radial variations in $\vec{\xi}$ may imply that the local linear approximations of adjacent magnetic surfaces overlap. These sharp variations are in fact typical of the ideal-MHD response near mode-rational surfaces; for example, ξ is generally discontinuous at these surfaces for ideal kink modes (when plasma inertia is excluded). This implies the breakdown of the linear ideal model in these regions, which must be resolved either by nonlinear or non-ideal physics. It can easily be shown that the condition for this local 'overlap' *not* to occur is

$$\frac{d\xi_r}{dr} > -1, \tag{12}$$

where ξ_r is the component of $\vec{\xi}$ normal to the equilibrium magnetic field, and r is the coordinate in this direction. For a linear calculation that includes a single toroidal mode number, so that $\xi_n \sim e^{in\phi}$, the violation of the condition

$$\left|\frac{d\xi_r}{dr}\right| < 1, \tag{13}$$

implies the that the local overlap condition (equation (12)) is violated at some toroidal angle for a given poloidal location.

Because the physical model in M3D-C1 is not ideal-MHD, the local linear displacement of magnetic surfaces is not generally well-defined. However, in the limit that $\vec{B} \cdot \nabla T_e = 0$, the linear displacement may be related to the local displacement of the electron isotherms:

$$\xi_n = -\delta T_e / |\nabla T_{e0}|. \tag{14}$$

This definition is unambiguous and well-defined in non-ideal calculations (at least in regions where $\nabla T_{e0} \neq 0$), and is therefore the definition we use here. In a non-ideal simulation, equation (13) no longer strictly implies that magnetic surfaces overlap. Instead, given the definition in equation (14), the criterion equation (13) can be interpreted as the condition under which the local linear approximation to the electron isotherms are implied to overlap. Since the actual isotherms in the calculation results by definition do not overlap, the violation of equation (13) implies a breakdown in the local linear approximation.

The value of $|d\xi_r/dr|$ is plotted for the modelled response of discharges 117327 ($n = 1$) and 148712 ($n = 3$) in figure 8. Note that the criterion (equation (13)) is never strictly violated for 117327, though $|d\xi_r/dr|$ gets as large as ≈ 0.75 near the magnetic x-points and the outer midplane. In contrast, the response in much of the region outside $q = 3$ in 148712 is found to violate this condition, indicating that nonlinear or non-ideal effects are important there. Indeed, field-line integration shows significant stochasticity in this region, indicating that the response is far from ideal.

It can also be seen in figure 8 that equation (13) is also violated in an annulus in the core of 148712 at the $q = 1$ surface. This is due to the large internal response at this surface. A result of this type is expected for an ideal (or near-ideal) kink response, since ξ_r is discontinuous (or nearly so) at the mode-rational surface for such a mode. In the calculations, this mode
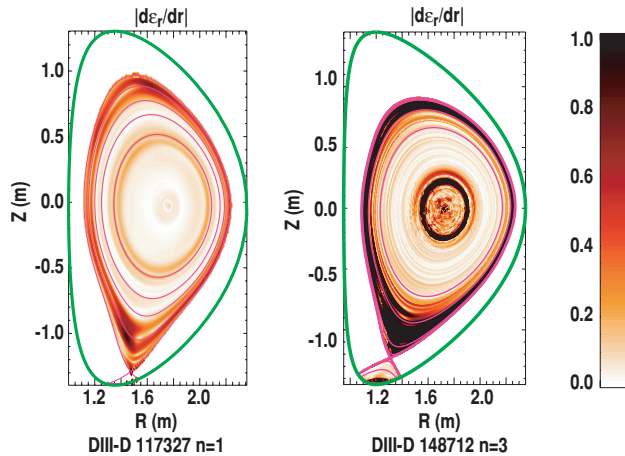
Figure 8. The value of $|d\xi_r/dr|$ is plotted for the modelled response of DIII-D discharges 117327 (left) and 148712 (right). The $q = 2$, 3, 4, and 5 surfaces and the LCFS are represented by the magenta curves. When $|d\xi_r/dr| \gtrsim 1$, nonlinear and/or non-ideal physics may play an important role in the response.

may be eliminated by raising q so that it never drops below one (by increasing the magnitude of the toroidal field, for example); doing this is found not to affect the edge response significantly in this case.

4. Discussion

Linear, two-fluid calculations of plasma response to applied non-axisymmetric fields have been carried out using M3D-C1. The calculated displacements of edge temperature profiles are found to be in good agreement with experimental measurements from Thomson scattering and soft x-ray diagnostics, in both phase and magnitude. The 3–4 cm peak-to-peak displacement found in the $n = 1$ case contrasts significantly with the calculated displacement of the separatrix manifolds due to the vacuum fields, which is approximately 0.72 cm at the Thomson chord in this case. These results underscore the importance of the plasma response in the determining edge displacements. Indeed, for the $n = 1$ case considered here it is found that the inclusion of both equilibrium rotation and two-fluid physics is crucial in obtaining quantitative agreement with the experimental measurements in both phase and magnitude. This is in contrast to some $n = 3$ cases in DIII-D, where the measured displacement is fairly well described by the vacuum separatrix manifold displacement [35].

An *a posteriori* investigation into the validity of the linearity of the response shows that this assumption is generally good throughout most of the plasma volume, but is often violated, or nearly violated, in the H-mode edge for equilibria and applied perturbations typical of DIII-D experiments. Seemingly unphysical features of some of the linear response hint at this breakdown; for example, the temperature becomes non-monotonic near the top of the pedestal at some toroidal angles in the $n = 3$ case, 148712 (see figure 4). It is likely that the predicted perturbations to the magnetic field are well-described by the linear model (with the possible exception of the resonant Fourier components of the field) even when the linearity of the density and

temperature response breaks down in the edge, since the magnetic field perturbations remain a small fraction of the total field everywhere. Nonlinear calculations using the same physical model must be carried out to quantify the error of these linear calculations. Nonlinear fluid calculations using physically realistic transport parameters are extremely challenging, though considerable progress towards this end has been made in recent years. Such calculations are underway, and will be compared directly to linear calculations in a future publication. Even if they are at the edge of their range of validity, the good agreement with experimental results shows that these linear calculations may still have good predictive capability in the plasma edge.

Aside from the issue of the breakdown of linearity, this numerical model, while relatively complete, relies on certain assumptions that could plausibly affect the results presented here. In particular, the boundary conditions used here are a perfectly conducting wall just within the position of the internal coils, which excludes the plasma response in the region exterior to the boundary. Since the frequency of the applied field is significantly lower than the current diffusion time of the vacuum vessel, the wall would probably be better modelled by a free boundary condition. We expect that the difference between the conducting wall and free boundary conditions will be relatively small when the plasma is far from the no-wall stability limit, but will become important as this limit is approached. Free boundary conditions are not yet possible in M3D-C1, but this issue will be addressed in the future when more flexible boundary conditions are implemented.

The two-fluid results presented here find that the plasma response typically acts to screen islands in the pedestal. The result of this is a considerable reduction in stochasticity, and the associated radial transport due to parallel diffusion, in that region. This resolves the apparent contradiction between vacuum modelling, which predicts significant radial diffusion of heat in the edge by parallel transport along stochastic field lines, and experiments, which do not consistently see a reduction of the temperature gradient upon application of magnetic perturbations. An exception to the screening effect occurs in regions where ω_e is small. In co-rotating plasmas, this region typically exists near the top of the H-mode pedestal, whereas in counter-rotating plasmas this condition is usually never met. This stochastization at the top of the pedestal is consistent with emerging experimental results [26], and may provide a mechanism for limiting the width of the pedestal to levels that are not unstable to ELMs in co-rotating plasmas [25]. In accordance with this hypothesis, ELM suppression by non-axisymmetric fields has not been definitively observed in counter-rotating plasmas.

It is worth noting that there remains uncertainty in the interpretation of the experimental results due to the lack of toroidally resolved measurements. Specifically, it is unknown whether and to what extent the phase-dependent temperature perturbations measured by Thomson scattering, for example, are due to a helical distortion of the plasma, or to an axisymmetric change in the underlying equilibrium. The method of rotating the toroidal phase of the applied fields to explore the non-axisymmetric structure of the plasma assumes that the underlying axisymmetric equilibrium is largely independent of the phase. However, axisymmetric

measures of the plasma equilibrium (such as line-averaged density and toroidal rotation) are found to be sensitive to the phase of the applied fields in practice. This indicates either the presence of significant error fields or the action of plasma control systems responding to toroidally localized measurements, neither of which are included in the M3D-C1 calculations. Two results presented here show that the phase dependence of the edge displacements are largely due to helical structures: first, the displacements calculated by M3D-C1, which are purely helical, are in good agreement with the observed displacements; and second, the poloidal structure of the x-ray emission is strongly indicative of field-aligned helical structures. Additional analysis of experimental measurements will be required to determine to what extent, and under what conditions, the helical response is greater than the axisymmetric response.

While these results indicate that the displacement is largely helical in character, the axisymmetric changes to the equilibrium induced by the application of non-axisymmetric fields—in particular, density pump-out and the braking of toroidal rotation—are often substantial, and may have important consequences for fusion energy output. Models of neoclassical toroidal viscosity that take into account the response of the plasma are now being used to estimate the torque expected from non-axisymmetric perturbations [36, 37]. Models of transport in non-axisymmetric fields are also under development [38–40]. Several of these models are presently being adapted to take the non-axisymmetric fields calculated with M3D-C1 as input, and are the subject of ongoing research. Ultimately, a quantitative understanding of the effect of non-axisymmetric perturbations on transport will likely be necessary to obtain a predictive model of ELM suppression by non-axisymmetric fields.

Acknowledgments

References

[1] Garofalo A.M. *et al* 2008 *Phys. Rev. Lett.* **101** 195005
[2] Evans T.E. *et al* 2004 *Phys. Rev. Lett.* **92** 235003
[3] McCool S.C. *et al* 1989 *Nucl. Fusion* **29** 547
[4] Vallet C. *et al* 1991 *Phys. Rev. Lett.* **67** 2662
[5] Buttery R.J. *et al* 2011 *Nucl. Fusion* **51** 073016
[6] Evans T.E., Roeder R.K.W., Carter J.A. and Rapoport B.I. 2004 *Contrib. Plasma Phys.* **44** 235
[7] Wingen A., Evans T.E. and Spatschek H. 2009 *Nucl. Fusion* **49** 055027
[8] Kirk A., Harrison J., Liu Y., Nardon E., Chapman I.T., Denner P. and the MAST Team 2012 *Phys. Rev. Lett.* **108** 255003
[9] Shafer M.W., Unterberg E.A., Orlov D.M., Evans T.E., Harris J.H., Hillis D.L., Maingi R., Moyer R.A., Nazikian R. and Wingen A. 2012 *Nucl. Fusion* **52** 122001
[10] Moyer R.A., Van Zeeland M.A., Orlov D.M., Wingen A., Evans T.E., Ferraro N.M., Hanson J.M., Nazikian R. and Wade M.R. 2012 *Nucl. Fusion* **52** 123019
[11] Fundamenski W., Pitts R.A. and JET EFDA Contributors 2007 *J. Nucl. Mater.* **363–365** 319
[12] Loarte A. 2012 private communication
[13] Jardin S.C., Ferraro N., Luo X., Chen J., Breslau J., Jansen K.E. and Shepard M.S. 2008 *J. Phys.: Conf. Series* **125** 012044
[14] Breslau J., Ferraro N. and Jardin S. 2009 *Phys. Plasmas* **16** 092503
[15] Ferraro N.M. 2012 *Phys. Plasmas* **19** 056105
[16] Park J.-K., Boozer A.H. and Glasser A.H. 2007 *Phys. Plasmas* **14** 052110
[17] Liu Y., Kirk A. and Nardon E. 2010 *Phys. Plasmas* **17** 122502
[18] Liu Y.Q., Bondeson A., Fransson C.M., Lennartson B. and Breitholtz C. 2000 *Phys. Plasmas* **7** 3681
[19] Luxon J.L. 2002 *Nucl. Fusion* **42** 614
[20] Roeder R.K.W, Rapoport B.I. and Evans T.E. 2003 *Phys. Plasmas* **10** 3796
[21] Fitzpatrick R. *et al* 1993 *Nucl. Fusion* **33** 1049
[22] Waelbroeck F.L. 2009 *Nucl. Fusion* **49** 104025
[23] Heyn M.F., Ivanov I.B., Kasilov S.V., Kernbichler W., Joseph I., Moyer R.A. and Runov A.M. 2008 *Nucl. Fusion* **48** 024005
[24] Nardon E., Tamain P., Bécoulet M., Huysmans G. and Waelbroek F.L. 2010 *Nucl. Fusion* **50** 034002
[25] Snyder P.B. *et al* 2012 *Phys. Plasmas* **19** 056115
[26] Wade M.R. 2012 *Proc. 24th Int. Conf. on Fusion Energy 2012 (San Diego, CA, 2012)* (Vienna: IAEA) CD-ROM file EX/3-1 and www-naweb.iaea.org/napc/ physics/index.html
[27] Burrell K.H., Gohil P., Groebner R.J., Kaplan D.H., Robinson J.I. and Solomon W.M. 2004 *Rev. Sci. Instrum.* **75** 3455
[28] Carlstrom T.N., Campbell G.L., DeBoo J.C., Evanko R. and Evans J. 1992 *Rev. Sci. Instrum.* **63** 4901
[29] Eldon D. *et al* 2012 *Rev. Sci. Instrum.* **83** 10E343
[30] Groebner R.J. *et al* 2001 *Nucl. Fusion* **41** 1789
[31] Shafer M.W., Battaglia D.J., Unterberg E.A., Canik J.M., Evans T.E., Harris J.H. and Meitner S.J. 2011 *Plasma Fusion Res.* **6** 2402041
[32] Fitzpatrick R. and Hender T.C. 1991 *Phys. Fluids* B **3** 644
[33] Schaffer M.J., Menard J.E., Aldan M.P., Bialek J.M., Evans T.E. and Moyer R.A. 2008 *Nucl. Fusion* **48** 024004
[34] Hudson S.R. and Breslau J. 2008 *Phys. Rev. Lett.* **100** 095001
[35] Orlov D.M., Evans T.E., Moyer R.A., Schaffer M.J., Schmitz O. and Loarte A. 2012 *Fusion Eng. Des.* **87** 1536
[36] Park J.-K. *et al* 2009 *Phys. Plasmas* **16** 056115
[37] Kim K., Park J.-K., Kramer G.J. and Boozer A.H. 2012 *Phys. Plasmas* **19** 082503
[38] Callen J.D., Cole A.J., Hegna C.C., Mordijck S. and Moyer R.A. 2011 *Technical Report* UW-CPTC11-13R, University of Wisconsin-Madison
[39] Bird T.M. and Hegna C.C. 2013 *Nucl. Fusion* **53** 013004
[40] Callen J.D., Cole A.J. and Hegna C.C. 2012 *Phys. Plasmas* **19** 112505